

HETE Observations of the Gamma-Ray Burst GRB030329: Evidence for an Underlying Soft X-ray Component

R. Vanderspek,¹ T. Sakamoto,^{2,3,4} C. Barraud,⁵ T. Tamagawa,³ C. Graziani,⁶ M. Suzuki,²
Y. Shirasaki,^{3,7} G. Prigozhin,¹ J. Villasenor,¹ J. G. Jernigan,⁸ G. B. Crew,¹ J.-L. Atteia,⁵
K. Hurley,⁸ N. Kawai,^{2,3} D. Q. Lamb,⁶ G. R. Ricker,¹ S. E. Woosley,⁹ N. Butler,¹
J. P. Doty,¹ A. Dullighan,¹ T. Q. Donaghy,⁶ E. E. Fenimore,⁴ M. Galassi,⁴ M. Matsuoka,¹⁰
K. Takagishi,¹¹ K. Torii,^{3,12} A. Yoshida,^{3,13} M. Boer,⁵ J.-P. Dezalay,¹⁴ J.-F. Olive,¹⁴
J. Braga,¹⁵ R. Manchanda,¹⁶ and G. Pizzichini¹⁷

ABSTRACT

An exceptionally intense gamma-ray burst, GRB030329, was detected and localized by the instruments on board the High Energy Transient Explorer satellite (*HETE*) at 11:37:14 UT on 29 March 2003. The burst consisted of two ~ 10 s pulses of roughly equal brightness and an X-ray tail lasting >100 s. The energy fluence in the 30–400 keV energy band was $S_\gamma = 1.2 \times 10^{-4}$ erg cm $^{-2}$, making

¹Center for Space Research, Massachusetts Institute of Technology, 70 Vassar Street, Cambridge, MA, 02139.

²Department of Physics, Tokyo Institute of Technology, 2-12-1 Ookayama, Meguro-ku, Tokyo 152-8551, Japan.

³RIKEN (Institute of Physical and Chemical Research), 2-1 Hirosawa, Wako, Saitama 351-0198, Japan.

⁴Los Alamos National Laboratory, P.O. Box 1663, Los Alamos, NM, 87545.

⁵Laboratoire d’Astrophysique, Observatoire Midi-Pyrénées, 14 Ave. E. Belin, 31400 Toulouse, France.

⁶Department of Astronomy and Astrophysics, University of Chicago, 5640 South Ellis Avenue, Chicago, IL 60637.

⁷National Astronomical Observatory, Osawa 2-21-1, Mitaka, Tokyo 181-8588 Japan.

⁸University of California at Berkeley, Space Sciences Laboratory, Berkeley, CA, 94720-7450.

⁹Department of Astronomy and Astrophysics, University of California at Santa Cruz, 477 Clark Kerr Hall, Santa Cruz, CA 95064.

¹⁰Tsukuba Space Center, National Space Development Agency of Japan, Tsukuba, Ibaraki, 305-8505, Japan.

¹¹Faculty of engineering, Miyazaki University, Gakuen Kibanadai Nishi, Miyazaki 889-2192, Japan.

¹²Department of Earth and Space Science, Graduate School of Science, Osaka University, 1-1 Machikaneyama-cho, Toyonaka, Osaka 560-0043, Japan.

¹³Department of Physics, Aoyama Gakuin University, Chitosedai 6-16-1 Setagaya-ku, Tokyo 157-8572, Japan.

¹⁴Centre d’Etude Spatiale des Rayonnements, Observatoire Midi-Pyrénées, 9 Ave. de Colonel Roche, 31028 Toulouse Cedex 4, France.

¹⁵Instituto Nacional de Pesquisas Espaciais, Avenida Dos Astronautas 1758, São José dos Campos 12227-010, Brazil.

¹⁶Department of Astronomy and Astrophysics, Tata Institute of Fundamental Research, Homi Bhabha Road, Mumbai, 400 005, India.

¹⁷Consiglio Nazionale delle Ricerche, IASF, Sezione di Bologna, via Piero Gobetti 101, 40129 Bologna, Italy.

GRB030329 one of the brightest GRBs ever detected. Communication of a $2'$ error box 73 minutes after the burst allowed the rapid detection of a counterpart in the optical, x-ray, radio and the ensuing discovery of a supernova with most unusual characteristics. Analyses of the burst lightcurves reveal the presence of a distinct, bright, soft X-ray component underlying the main GRB: the 2–10 keV fluence of this component is $\sim 7 \times 10^{-6}$ erg cm^{-2} . The main pulses of GRB030329 were preceded by two soft, faint, non-thermal bumps. We present details of the *HETE* observations of GRB030329.

Subject headings: gamma rays: bursts (GRB030329)

1. Introduction

On March 29, 2003 the High Energy Transient Explorer (*HETE*; Ricker et al. (2003)) detected one of the brightest gamma-ray bursts ever recorded, GRB030329. The intense flux of this burst and the special characteristics of the *HETE* mission allowed the $2'$ localization of the burst to be communicated worldwide 72 minutes after the onset of the burst. This led, in turn, to the rapid discovery of optical, x-ray, and radio counterparts to the burst, and, about one week later, to the discovery of one of the most energetic, unusual supernovae ever observed, SN 2003dh (Stanek et al. 2003; Hjorth et al. 2003). This watershed event showed conclusively that at least some long GRBs occur in conjunction with supernovae. Such an association was predicted by the collapsar model (Woosley 1993; MacFadyen & Woosley 1999).

The instruments on *HETE* allow the study of prompt radiation down to energies as low as 2 keV. The combination of high flux and low energy sensitivity has allowed us to carry out very detailed analyses of the prompt emission of GRB030329. These analyses have revealed soft features in the lightcurve: faint, non-thermal, soft X-ray “bumps” before the main GRB and a bright, soft X-ray component underlying the main GRB. In this paper, we describe the *HETE* observations of the prompt emission of GRB030329.

2. Discovery

GRB030329 was detected by the *HETE* satellite (Ricker et al. 2003) as trigger H2652 at 11:37:14.7 UT (41834.7 SOD) on March 29, 2003 (Vanderspek et al. 2003). GRB030329 was seen as a very bright double-pulsed burst with a duration of over 100s in all three *HETE* instruments: Fregate: 7–400 keV (Atteia et al. 2003); Wide-field X-ray Monitor (WXM):

2–25 keV (Shirasaki et al. 2003); Soft X-ray Camera (SXC): 2–10 keV (Villasenor et al. 2003). GRB030329 had a 30–400 keV fluence of $S_\gamma = 1.18 \times 10^{-4}$ erg cm $^{-2}$, making it one of the brightest GRBs detected by *HETE* to date and placing it among the top 1% of the brightest GRBs ever detected. The burst duration was $t_{90} = 22.9$ s at high energies (30–400 keV), increasing to $t_{90} \approx 38$ s at low energies (2–10 keV); a soft X-ray tail is seen extending >100 seconds after burst onset.

The burst was localized by the SXC to a 2' radius error circle (90%) centered at $\alpha = 10^h 44^m 49^s$, $\delta = +21^\circ 28' 44''$ (J2000): this position was distributed to the GRB Coordinates Distribution Network (GCN) 73 minutes after the burst. Torii (2003) began optical observations of the SXC error region less than two minutes after the distribution of the GCN Notice, Peterson & Price (2003) fifteen minutes later; both observations revealed a bright ($R < 13$) optical transient (OT) just outside the SXC error circle. The bright OT was monitored by many observers over the following days (Uemura 2003; Smith et al. 2003; Gal-Yam et al. 2003; Klose et al. 2003; Burenin et al. 2003; Lipunov et al. 2003; Price et al. 2003). Greiner et al. (2003) reported a redshift of 0.1685, making GRB030329 the closest GRB with a measured redshift after GRB980425 (Lidman et al. 1998; Tinney, Stathakis & Cannon 1998) and GRB031203 (Prochaska et al. 2003; Watson et al. 2004). The emergence of the signature of a type Ic supernova from the spectrum of the optical counterpart (Matheson et al. 2003; Stanek et al. 2003; Hjorth et al. 2003) solidifies the association of some GRBs with core-collapse supernovae.

Prompt followup observations revealed the enormous brightness of GRB030329 at other wavelengths. An RXTE observation of the X-ray afterglow starting less than five hours after the burst revealed the source to have a 2–10 keV flux of 1.4×10^{-10} erg cm $^{-2}$ s $^{-1}$, one of the brightest GRB X-ray afterglows ever measured (Marshall & Swank 2003). VLA observations at 8.46 GHz fourteen hours after the burst (Berger et al. 2003) revealed a 3.5 mJy source, the brightest radio afterglow yet measured. The brightness of the radio afterglow was confirmed in the days following the burst at a wide range of radio wavelengths (Pooley 2003; Pramesh Rao et al. 2003; Hoge et al. 2003; Kuno et al. 2003; Finkelstein et al. 2003). GRB030329 was also detected as a Sudden Ionospheric Disturbance (Schnoor et al. 2003), as the incoming X-ray flux was sufficiently strong to create a global surge in the electron density on the illuminated side of the Earth.

3. Observations

GRB030329 was detected by Fregate as an 8.3σ excess in the 7–80 keV band on the 1.3s timescale trigger. This excess was due to a soft, relatively weak precursor: thirteen seconds

later, the burst was as bright as any seen during the *HETE* mission. Real-time reports of the burst brightness via the *HETE* VHF system (Crew et al. 2003) showed the significance of the burst in the WXM exceeding the 7 bits allotted in the telemetry stream at $S/N=127$. At the same time, the image S/N reported from the WXM was 60, twice that of the previous brightest burst (GRB020813).

Ground analyses of the downlinked data starting ~ 40 minutes after the trigger confirmed the magnitude of the burst. The burst was detected at a S/N of over 300 in both *Fregate* and the WXM, and over 100 in the SXC: this burst is the brightest *HETE* has detected in the 7–80 keV band. Unfortunately, the burst was *so* bright and *so* long that the *Fregate* flight software decided the burst was due to a increase in the overall background rate and “invalidated” the burst in flight. As a result, the initial real-time GCN messages indicated that H2652 was *not* a real GRB. More important, however, is the fact that time-tagged photons are not downlinked from the *Fregate* instrument for bursts that are invalidated in flight¹. The temporal and spectral analyses of *Fregate* data were therefore done with survey data: lightcurves in three broad energy bands (band A: 7–40 keV; band B: 7–80 keV; band C: 30–400 keV) at 80 ms time resolution and 128-channel spectral data products with a time resolution of 5.2 seconds.

3.1. Localization

GRB030329 was very bright in X-rays: the burst was detected at a S/N of 350 in the WXM. However, the large incident angle of the burst was such that only one of the two X detectors and one of the two Y detectors of the WXM were illuminated. Unfortunately, the Y detector illuminated by the burst was YB, which was lost due to a micrometeorite impact in January 2003; as a result, while the WXM could be used to determine the X position very precisely, the Y position could only be crudely determined, based on the relative illumination of the six wires in the X detectors. Fortunately, despite the large incident angle, GRB030329 was well detected in both the SXC X and Y detectors.

The real-time localization of GRB030329 calculated in flight reflected these facts: the image S/N calculated on board (which reflects the strength of the peak in the cross-correlation map) was 60 in X, but less than 2 in the Y direction. As the SXC flight imaging software, which looks for significant cross-correlation peaks near the WXM localization, requires image

¹This same scenario occurred 24 hours earlier on the bright burst GRB030328 (H2650), the only two times in the course of the *HETE* mission that real GRBs have been invalidated in flight. The flight software has since been modified to prevent bright bursts from being invalidated.

S/N values greater than 3 in both WXM axes to proceed, no real-time SXC localization was available.

Ground analyses of the WXM and SXC data began after the full data set was down-linked, at 12:10 UT (33 minutes after the burst). It quickly became clear that only the X detector was illuminated, limiting the WXM localization to a box measuring $12' \times 2.25^\circ$. Fortunately, the burst was so bright in the SXC that it was possible to calculate a position without reference to the WXM position, and the SXC position was in the WXM error box. The SXC localization was distributed by GCN Notice at 12:50 UT (73 minutes after the burst) as a $2'$ circle centered on $\alpha = 10^h 44^m 49^s$, $\delta = +21^\circ 28' 44''$ (J2000). Continued analyses of the SXC data after the distribution of the first GCN Notice revealed that a correction to the localization to account for systematic errors at large incident angles had not been applied, and that the procedure to distribute such localizations with a larger quoted error circles had not been followed. A revised error region that compensates for the systematic error was distributed in Vanderspek et al. (2003): it is a $2'$ circle centered on $\alpha = 10^h 44^m 50^s$, $\delta = +21^\circ 30' 54''$ (J2000). The skymap of GRB030329, showing the WXM and SXC localizations and the OT, is shown in Figure 1.

GRB030329 was observed by every spacecraft in the Interplanetary Network (Ulysses, Konus-Wind, Mars Odyssey (HEND and GRS), RHESSI, and INTEGRAL (SPI-ACS)) and the resulting IPN localization is fully consistent with, but does not constrain, the WXM and SXC localizations (K. Hurley 2003, private communication).

3.2. Temporal Properties

As shown in Figure 2, the time profile of GRB030329 is dominated by two strong pulses separated by 11s and an extended soft tail that continues >60 seconds after the trigger. The Fregate band D ($E > 400$ keV) lightcurve shows a $\sim 6\sigma$ enhancement over background during the first pulse and a single 80 ms bin “spike” at $t=26.2$ s, coincident with the peak of the second pulse. The burst duration was $t_{90} = 22.9$ s at high energies (30–400 keV), increasing to $t_{90} \approx 38$ s at low energies (2–10 keV): Table 1 gives the T_{50} and T_{90} durations for various SXC, WXM and FREGATE energy bands (Kouveliotou et al. 1993). Both duration measures decrease with increasing energy: this behavior is typical of many long-duration GRBs (Fenimore et al. 1995).

There is clear spectral evolution during the burst, as the relative brightness of the first pulse to the second pulse is larger in Fregate band C than in band A. There is also distinctly different spectral behavior in the two pulses. In Figure 3, we overlay the SXC (2–10 keV) and

Fregate band C lightcurves: while the onset of the second pulse is essentially simultaneous in all energy bands, there is a delay in the peak of the first pulse of ~ 5 seconds between photons with $E > 25$ keV and those with $E < 10$ keV. The nature of this evolution is discussed in more detail in Section 4.1.

The inset figures of Figure 2 reveal two small precursor bumps, seen primarily in Fregate bands A and B. (The second bump in band B is in fact the trigger for this burst in Fregate). While the bumps are not as significant in the WXM and SXC lightcurves, localization analyses of both WXM and SXC data show the photons came from the same celestial coordinates as the photons from the two main pulses: this result holds for photons detected as early as $t = -13$ s. Integrating a pair of gaussians fit to the two bumps shows that the total counts in the two bumps is roughly 1% of the total in the two main pulses in both bands A and B. In each bump, the 7–30 keV counts fluence is $\sim 90\%$ of the 7–80 keV counts fluence, indicating that the bulk of the precursor emission is < 30 keV; the fact that the second bump is slightly more prominent than the first one in band C (see the inset of 2b) may indicate that the second bump is somewhat harder than the first. Also visible in the inset figures in Figure 2 is a general rise in the count rates at lower energies in the period leading up to the first major pulse. The burst begins in the 30–400 keV band at $t \approx -4$ seconds, while 2–25 keV photons are first detected at $t \approx -13$ seconds.

GRB030329 also has a soft X-ray tail which continues > 100 s after the trigger. T. Tamagawa et al (2004, private communication) have shown that an extrapolation of the 2–10 keV photon energy flux of the afterglow (Tiengo et al. 2003; Marshall et al. 2003) back to $t=100$ s is consistent with the 2–10 keV photon energy flux observed in the X-ray tail at that time; the spectral index of the tail (~ -2.1) is also consistent with that cited in Tiengo et al. (2003). The soft X-ray tail of GRB 030329 will be discussed in more detail in Atteia et al. (2004).

3.3. Spectrum

Because the burst was invalidated in flight, there are no time-tagged photon data from the Fregate instrument available. However, survey spectral data, which consists of 128 spectral bins every 5.2 seconds, can be used to calculate the burst spectral parameters. The spectrum of the entire burst can be well fit by a Band function from 2–400 keV, with parameters $\alpha = -1.32 \pm 0.02$, $\beta = -2.44 \pm 0.08$, and $E_{peak} = 70.2 \pm 2.3$ (errors are 90%); however, in time-resolved spectroscopy, these parameters vary significantly during the course of the burst. The burst fluence was $S_\gamma = 1.2 \times 10^{-4}$ erg cm^{-2} in the 30–400 keV band, $S_X = 5.5 \times 10^{-5}$ erg cm^{-2} in the 2–30 keV band: the hardness ratio S_X/S_γ is 0.56, which

qualifies GRB030329 as an X-ray rich burst (Heise et al. 2001). At the measured redshift of 0.1685, the total isotropic energy released was $(1.86 \pm 0.08) \times 10^{52}$ erg and E_{peak} in the source frame is 82.0 ± 2.6 keV, consistent with the relationship described in Amati et al. (2002). The time-integrated emission properties of GRB030329 in various energy bands are given in Table 2.

The results of time-resolved spectral analyses are given in Table 3 and plotted in Figure 4. The Fregate and WXM data were fit jointly, to a Band function when possible and a power-law model when a significant value of Band β could not be calculated. The data show a strong softening of the burst spectrum during the course of the first pulse, followed by a mild re-hardening at the onset of the second pulse and a subsequent softening.

Power-law fits to the WXM precursor data reveal that the photon indices of the two bumps are similar, -2.0 ± 0.4 . A joint fit of a power-law model to the WXM and Fregate data for both bumps together (from $t=-13$ s to $t=+3$ s) shows a photon index of -2.11 ± 0.09 , a 2–25 keV fluence of 1.2×10^{-6} erg cm^{-2} , and a 30–400 keV fluence of 9.3×10^{-7} erg cm^{-2} . (Fits of the precursor data to a cutoff power law (Comptonization) model and a Band function were also performed, but neither resulted in a significant improvement in χ^2). The power-law fit is quite good (reduced χ^2 of 0.7): the precursor spectra are very clearly non-thermal.

4. Soft X-Ray Emission and Precursor Activity

4.1. Spectral Lag or Soft X-ray Bump?

At first glance, the broadband lightcurves shown in Figure 2 seem to indicate that there is a strong hard-to-soft evolution in the burst emission in the first pulse. However, closer evaluation of the burst lightcurves suggests that this “evolution” is more likely due to a relatively bright, soft X-ray bump of ~ 20 seconds duration centered at $t \approx 20$ s after the burst trigger, as shown in the overlay of band C and SXC emission in Figure 3.

We examined the GRB030329 burst data for spectral lags of the type discussed in Band (1997). This analysis was made difficult because the Fregate broadband lightcurve bandpasses do not match up well with the BATSE discriminator bandpasses (20–50 keV, 50–100 keV, 100–300 keV) and because there are no time-tagged photon data with which to reconstruct such lightcurves; however, linear combinations of Fregate bandpass lightcurves can be used to shed some light on the spectral evolution of the first pulse of the burst. We calculate the difference of Fregate band B (7–80 keV) and Fregate band A (7–40 keV) to create a Fregate band “B-A” with an effective bandpass of 40–80 keV; we also construct a “C-(B-A)” lightcurve, which has an effective energy bandpass of 30–40 keV *plus* 80–400 keV.

A simple cross-correlation of the band B-A lightcurve with the band C-(B-A) lightcurve (160 ms time resolution) shows a “lag” of 6 ± 32 milliseconds. This value indicates that there is essentially no shift in the temporal structure of the GRB030329 lightcurve with energy at energies greater than 30 keV, and thus that the strong spectral evolution in the first pulse must be due to photons with $E < 30$ keV.

As an alternate approach to understanding the temporal and spectral variability of the main pulses, we scale the B-A lightcurve to the C-(B-A) lightcurve and examine the differences between the two. The scaling is done using only the data at the peak of the first pulse (between $t=14.5$ s and $t=15.5$ s after the trigger): the resultant scale factor is 0.42. In Figure 5 we show the band C-(B-A) lightcurve, the scaled band B-A lightcurve, and the difference between the two: the shapes of the lightcurves match extremely well for the duration of the burst, even though the scaling was done using data only from the maximum of the first pulse. The difference reflects differences in the temporal characteristics of the [30–40] + [80–400] keV band with respect to the template 40–80 keV band and could be due to features in either the 30–40 keV band or the 80–400 keV band. The difference is consistent with zero except for a few pulse-like features - - most notable are a peak at $t=20$ s, consistent with the peak of the soft X-ray emission (Figure 3), a peak at the start of the second pulse ($t=25$ s), and a spike coincident with the band D spike ($t=26$ s) - - and a faint tail starting at $t=28$ s. Interpretation of the details of this difference is not straightforward; however, this analysis confirms that the extreme “lag” implied by the lightcurves in Figures 2 and 3 is not seen at energies >30 keV.

The more likely explanation for the time profiles seen in Figures 2 and 3 is a bump of soft X-ray emission which begins at about the same time as the main GRB and peaks at $t \approx 20$ s, five seconds after the peak of the first pulse. Analysis of the 2–10 keV lightcurve show that a gaussian with a FWHM of ~ 12 seconds is a reasonable fit to that pulse: we estimate the 2–10 keV fluence of this pulse to be $\sim 7 \times 10^{-6}$ erg cm^{-2} (because the spectrum of GRB itself extends into the soft X-ray band, it is not possible to clearly separate the first pulse into the sum of two distinct lightcurves).

Detailed spectral analyses of the soft X-ray pulse are made difficult by the overlap with the first GRB pulse and the absence of high-time-resolution spectral data; thus, it is not possible to demonstrate the existence of the soft X-ray pulse by fitting the spectrum of GRB030329 to a two-component spectral model. The excellent fit of the burst spectrum to a GRB model (Band et al. 1993) in that time period indicates that the soft pulse likely has a non-thermal spectrum. If the broadband lightcurve data are not considered, it would be easy to disregard this soft emission as part of the spectral evolution of the GRB; however, the dissimilarity in the 2–10 keV and band C lightcurves in the first pulse and the stark

contrast in the burst emission profiles above 30 keV vs. below 20 keV strongly suggest that the soft X-ray pulse is indeed a distinct emission component.

The behavior of the soft X-rays of the second pulse is entirely different from that of the first pulse. The fast rise of the 2–10 keV count rate in the second pulse is coincident with the onset of the second pulse in the band C lightcurve, in contrast to the delayed rise of the 2–10 keV component of the first pulse. There is no evidence for a distinct soft X-ray component in the second pulse: the similarity of the band C and 2–25 keV time profiles in the second pulse indicates that the emission in these two bands likely come from the same source, with any variations in relative brightness being due to spectral parameters changing as a function of time (see Figure 4).

4.2. Precursors

The concept of a burst “precursor” has various definitions when applied to GRBs. The original definitions were ostensibly “ γ -rays seen before the pulse that triggered the instrument” or “X-rays seen before the γ -rays”. The term “precursor” has been applied to γ -ray pulses before the event that triggered BATSE (Koshut et al. 1995), the slow onset of soft X-ray emission before the main γ -ray pulse (e.g., GRB900623; Murakami et al. (1991)), as well as isolated X-ray pulses before the GRB itself (e.g., GRB790307, Laros et al. (1984)).

Koshut et al. (1995) defined a precursor to be emission which precedes the main burst by at least the duration of the main burst; using this restrictive definition and BATSE DISCLA data with $E > 25$ keV, they found that the distribution of “precursor” spectral parameters is not significantly different than the distribution of GRB spectral parameters. On the other hand, in ’t Zand et al. (1999) distinguish precursor emission from the burst emission by *requiring* that the precursor emission be described by an entirely different spectral model than the burst emission or that the spectral parameters of the precursor be unprecedented in describing GRBs in the γ -ray phase. According to in ’t Zand et al., then, the thermal emission of GRB900126 (Murakami et al. 1991) is a true precursor, while the “X-ray bumps before the GRB” in GRB980519 and GRB990704 (Feroci et al. 2001) are not. Koshut et al. would not consider any of these examples to be true precursors; however, these precursors are so soft that they would not have been considered in their analysis.

The features in the low-energy lightcurves of GRB030329 at $t \approx -10$ s and $t \approx 2$ s are very similar to the “X-ray bumps before the GRB” in GRB980519. In that burst, detected by BeppoSAX, three soft X-ray bumps precede the main burst by 10–40 seconds; the bumps are non-thermal and are well-fit by a power law of index ~ -2 : in ’t Zand et al. (1999)

consider these bumps to be part of the main burst emission. In fact, the spectral evolution of GRB980519 overall is quite similar to that of GRB030329, as the power-law index is ~ -1 at the peak of the burst, then settles to values near -2 as the burst fades. GRB980519 is significantly fainter, however: the 25–300 keV fluence is 7×10^{-6} erg cm^{-2} , roughly fifteen times fainter than GRB030329. Scaling from Figure 2 of in 't Zand et al. (1999), the 2–10 keV fluence of the “X-ray bumps before the GRB” of GRB980519 is $\sim 5 \times 10^{-7}$ erg cm^{-2} , which, for a power law of index -2 , is comparable to the 2–25 keV fluence of $\sim 10^{-6}$ erg cm^{-2} for GRB030329. It is unclear whether the fact that these pre-GRB X-ray fluences are so similar for bursts that differ by $> 10\times$ in overall fluence is an indication that an independent mechanism is responsible for the creation of the pre-GRB X-rays; the detection of more bursts of this kind are required to understand this better. Several bursts in the HETE database have similar X-ray “precursors”: these will be discussed in a separate paper.

5. Conclusions

GRB030329 was seen as a two-peaked GRB with $S_\gamma = 1.2 \times 10^{-4}$ erg cm^{-2} , making it the brightest GRB detected by HETE and one of the brightest GRBs ever detected. The substantial X-ray fluence of GRB030329 (5.5×10^{-5} erg cm^{-2}) puts it in the class of X-ray Rich GRBs. The overall burst can be fit with a GRB model, with $\alpha = -1.32 \pm 0.02$, $\beta = -2.44 \pm .08$, and $E_{peak} = 70.2 \pm 2.3$ keV, but there is substantial spectral variability during the burst.

Detailed analyses of the burst lightcurves reveal the presence of a soft X-ray component distinct from the main GRB. This component consists almost entirely of photons with energies < 25 keV, and it is quite bright: the 2–10 keV fluence is $\sim 7 \times 10^{-6}$ erg cm^{-2} . The burst lightcurves also show two soft, non-thermal X-ray “precursor” bumps; while such pre-gamma-ray peak X-ray emission has been detected in some GRBs, it is not a common feature of GRB lightcurves.

The enormous brightness of the optical afterglow of GRB030329 has allowed it to be used as a “Rosetta Stone” in understanding the correlation of GRBs with Type Ic supernovae. The analysis of the bright prompt X- and γ -ray emission of GRB030329 has revealed a bright, soft X-ray component apparently uncorrelated with the main body of the burst emission. The obvious presence of this feature in a burst as bright as GRB030329 leads to the question of whether this feature is present in other GRBs and whether the brightness of the feature scales with burst fluence. This underlying soft pulse would not have been detected by the BATSE LADs, as detectors sensitive to photons with $E < 20$ keV are required to detect these pulses; however, at certain gain settings, the BATSE SDs would have detected the soft

emission of such an intense event (Preece et al. 2000). Searches for such features in GRBs detected by HETE are underway; we urge that similar analyses of BeppoSAX, Ginga, and BATSE SD data be performed. In this way, perhaps GRB030329 will also act as a “Rosetta Stone” in furthering our understanding of the prompt X- and γ -ray emission in long GRBs.

Acknowledgments

The authors acknowledge useful discussions with Enrico Ramirez-Ruiz, Chryssa Kouveliotou, Jay Norris, Jon Hakkila, Marco Feroci, and Filippo Frontera. The authors also thank the referee for a thorough reading of the manuscript and several insightful comments. The HETE mission is supported in the US by NASA contract NASW-4690; in Japan, in part by the Ministry of Education, Culture, Sports, Science, and Technology Grant-in-Aid 13440063; and in France, by CNES contract 793-01-8479. KH is grateful for HETE support under Contract MIT-SC-R-293291, for Ulysses support under JPL Contract 958056, and for IPN support under NASA grant FDNAG5-11451. SW is thankful for support under the NASA Theory Program under grant NAG5-12036. G. Pizzichini acknowledges support by the Italian Space Agency.

REFERENCES

- Amati, L. et al. 2002, *A & A*, 390, 81
- Atteia, J-L. et al. 2003, in *Gamma-Ray Burst and Afterglow Astronomy 2001*, AIP Conf. Proc 662, ed. G. R. Ricker & R. K. Vanderspek (New York: AIP), 17
- Atteia, J-L. et al. 2004, in preparation.
- Band, D. et al. 1993, *ApJ*, 413, 281
- Band, D. 1997, *ApJ*, 486, 928
- Berger, E., Soderberg, A. M., & Frail, D. A. 2003, *GCN Circ.* 2014 (<http://gcn.gsfc.nasa.gov/gcn/gcn3/2014.gcn3>)
- Burenin, R. et al. 2003, *GCN Circ.* 2001 (<http://gcn.gsfc.nasa.gov/gcn/gcn3/2001.gcn3>)
- Crew, G. B. et al. 2003, in *Gamma-Ray Burst and Afterglow Astronomy 2001*, AIP Conf. Proc 662, ed. G. R. Ricker & R. K. Vanderspek (New York: AIP), 66.

- Fenimore., E. E., in 't Zand, J. J. M., Norris, J. P., Bonnell, J. T. & Nemiroff, R. J. 1995, ApJ lett. 448, L101
- Feroci, M. et al. 2001, A&A, 378, 441
- Finkelstein, A. M., Ipatov, A. V., & Gnedin, Yu. N. 2003, GCN Circ. 2161 (<http://gcn.gsfc.nasa.gov/gcn/gcn3/2161.gcn3>)
- Gal-Yam, A., Ofek, E. O., Polishook, D., & Leibowitz, E. M. 2003, GCN Circ. 1999 (<http://gcn.gsfc.nasa.gov/gcn/gcn3/1999.gcn3>)
- Greiner, J. et al. 2003, GCN Circ. 2020 (<http://gcn.gsfc.nasa.gov/gcn/gcn3/2003.gcn3>)
- Heise, J., in 't Zand, J., Kippen, R.M., and Woods, P. 2001, in Gamma-Ray Bursts in the Afterglow Era, ESO Astrophysics Symposia (Berlin: Springer), 16
- Hjorth, J. et al. 2003, Nature, 423, 847
- Hoge, J. C., Meijerink, R., Tilanus, R. P. J., & Smith, I. A. 2003, GCN Circ. 2088 (<http://gcn.gsfc.nasa.gov/gcn/gcn3/2088.gcn3>)
- Klose, S., Hoegner, C., & Greiner, J. 2003, GCN Circ. 2000 (<http://gcn.gsfc.nasa.gov/gcn/gcn3/2000.gcn3>)
- Koshut, T. M., et al. 1995, ApJ, 452, 145.
- Kouveliotou, C., et al. 1993, ApJ, 413, L101.
- Kuno, N., Sato, N, & Nakanishi, H. 2003, GCN Circ. 2089 (<http://gcn.gsfc.nasa.gov/gcn/gcn3/2089.gcn3>)
- Laros, J. G. et al. 1984, ApJ, 286, 681
- Lidman, C. et al. 1998, IAUC Circ. 6895 (<http://cfa-www.harvard.edu/iauc/06800/06895.html>)
- Lipunov, V. et al. 2003, GCN Circ. 2002 (<http://gcn.gsfc.nasa.gov/gcn/gcn3/2002.gcn3>)
- MacFadyen, A., Woosley, S. E. 1999 ApJ, 524, 262
- Marshall, F. E. & Swank, J. H. 2003, GCN Circ. 1996 (<http://gcn.gsfc.nasa.gov/gcn/gcn3/1996.gcn3>)
- Marshall, F. E., Markwardt, C. & Swank, J. H. 2003, GCN Circ. 2052 (<http://gcn.gsfc.nasa.gov/gcn/gcn3/2052.gcn3>)

- Matheson, R. et al. 2003, GCN Circ. 2107 (<http://gcn.gsfc.nasa.gov/gcn/gcn3/2107.gcn3>)
- Murakami, T. et al. 1991, *Nature*, 350, 592.
- Peterson, B. A. & Price, P. A. 2003, GCN Circ. 1985 (<http://gcn.gsfc.nasa.gov/gcn/gcn3/1985.gcn3>)
- Pooley, G. 2003, GCN Circ. 2043 (<http://gcn.gsfc.nasa.gov/gcn/gcn3/2043.gcn3>)
- Pramesh Rao, A., Ishwara Chandra, C. H., & Bhattacharya, D. 2003, GCN Circ. 2073 (<http://gcn.gsfc.nasa.gov/gcn/gcn3/2073.gcn3>)
- Preece, R. D. et al. 2000, *ApJ Suppl.* 126, 19.
- Price, P. A. et al. 2003, *Nature*, 423, 844
- Prochaska, J. X. et al. 2003, GCN Circ. 2482 (<http://gcn.gsfc.nasa.gov/gcn/gcn3/2482.gcn3>)
- Ricker, G. R. et al. 2003, in *Gamma-Ray Burst and Afterglow Astronomy 2001*, AIP Conf. Proc 662, ed. G. R. Ricker & R. K. Vanderspek (New York: AIP), 3.
- Smith, D. et al. 2003 *ApJ* 596, L151.
- Schnoor, P. W., Welch, D. L., Fishman, G. J., and Price, A. 2003, GCN Circ. 2176 (<http://gcn.gsfc.nasa.gov/gcn/gcn3/2176.gcn3>)
- Shirasaki, Y. et al. 2003, *PASJ* 55, 1033
- Stanek, K. Z. et al. 2003, *ApJL*, 591, L17
- Tiengo, A., Mereghetti, S., Ghisellini, G., Rossi, E., Ghirlanda, G., & Schartel, N. 2003, *A&A*, submitted (astro-ph/0305564)
- Tinney, C., Stathakis, R., and Cannon, R. 1998, *IAUC Circ.* 6896 (<http://cfa-www.harvard.edu/iauc/06800/06896.html>)
- Torii, K. 2003, GCN Circ. 1986 (<http://gcn.gsfc.nasa.gov/gcn/gcn3/1986.gcn3>)
- Uemura, M. 2003, GCN Circ. 1989 (<http://gcn.gsfc.nasa.gov/gcn/gcn3/1989.gcn3>)
- Vanderspek, R. et al. 2003, GCN Circ. 1997 (<http://gcn.gsfc.nasa.gov/gcn/gcn3/1997.gcn3>)
- Villasenor, J. N. et al. 2003, in *Gamma-Ray Burst and Afterglow Astronomy 2001*, AIP Conf. Proc 662, ed. G. R. Ricker & R. K. Vanderspek (New York: AIP), 33.

Watson, S. E. 1993, ApJ, 605, L101.

Woosley, S. E. 1993, ApJ, 405, 273.

in 't Zand, J. J. M., Heise, J., van Paradijs, J., and Fenimore, E.E. 1999, ApJ, 516, L57

Table 1. Temporal Properties of GRB030329.

Instrument	Energy (keV)	T_{50} (s)	T_{90} (s)
HETE SXC	2–10	12.2 ± 0.3	34.7 ± 1.5
HETE WXM	2–25	12.8 ± 0.2	41.6 ± 0.8
	2–5	14.5 ± 0.4	52.1 ± 1.2
	5–10	12.4 ± 0.3	39.8 ± 1.0
	10–25	11.5 ± 0.2	36.9 ± 1.1
HETE FREGATE	7–40	11.2 ± 0.06	29.1 ± 0.6
	30–400	11.2 ± 0.05	22.8 ± 0.5

Note. — Errors are 1σ ; the SXC energy range is approximate.

Table 2. Emission Properties of GRB030329.

Energy (keV)	Photon Flux (ph cm ⁻² s ⁻¹)	Energy Flux (10 ⁻⁷ erg cm ⁻² s ⁻¹)	Energy Fluence (10 ⁻⁵ erg cm ⁻²)
2–10	57.5 ± 1.1	4.20 ± 0.07	2.64 ± 0.04
2–25	77.0 ± 1.1	9.16 ± 0.08	5.76 ± 0.05
2–30	79.9 ± 1.1	10.43 ± 0.08	6.57 ± 0.05
7–30	32.35 ± 0.19	7.53 ± 0.04	4.74 ± 0.03
30–400	15.09 ± 0.10	18.78 ± 0.25	11.82 ± 0.16
50–100	5.39 ± 0.05	5.98 ± 0.06	3.76 ± 0.04
100–300	2.91 ± 0.05	7.35 ± 0.16	4.62 ± 0.10

Note. — Errors are for 90% confidence. All values were calculated from the time-averaged Band spectrum of the entire burst.

Table 3. Spectral Model Parameters for GRB030329.

Time since trigger (s)	α^a	β	E_{peak} (keV)	2–25 keV Flux	30–400 keV Flux
-10.05 – -5.05 ^b	-2.16 ^{+0.38} _{-0.44}	0.66 ^{+0.18} _{-0.17}	...
-5.05 – -0.05 ^b	-1.96 ^{+0.49} _{-0.56}	0.68 ^{+0.23} _{-0.20}	...
-0.05 – 4.95 ^b	-2.01 ^{+0.31} _{-0.30}	1.18 ^{+0.24} _{-0.20}	...
4.95 – 9.95 ^b	-1.97 ^{+0.25} _{-0.27}	1.37 ^{+0.23} _{-0.22}	...
-12.85 – 2.95	-2.11 ^{+0.08} _{-0.09}	0.77 ^{+0.07} _{-0.07}	0.59 ^{+0.14} _{-0.12}
8.15 – 13.45	-1.27 ^{+0.05} _{-0.04}	-3.29 ^{+0.97} _{-6.71}	106.80 ^{+12.5} _{-11.9}	5.03 ^{+0.15} _{-0.15}	14.12 ^{+0.72} _{-0.67}
13.45 – 18.65	-0.89 ^{+0.02} _{-0.02}	-2.35 ^{+0.06} _{-0.08}	87.03 ^{+3.2} _{-3.0}	24.12 ^{+0.24} _{-0.26}	95.69 ^{+1.28} _{-1.27}
18.65 – 23.85	-1.27 ^{+0.04} _{-0.04}	-2.70 ^{+0.12} _{-0.20}	41.35 ^{+2.2} _{-2.0}	17.57 ^{+0.25} _{-0.23}	22.66 ^{+0.69} _{-0.73}
23.85 – 29.15	-1.15 ^{+0.03} _{-0.03}	-2.32 ^{+0.04} _{-0.06}	52.45 ^{+2.4} _{-2.0}	33.34 ^{+0.31} _{-0.30}	66.74 ^{+1.04} _{-1.04}
29.15 – 34.35	-1.67 ^{+0.02} _{-0.03}	-4.57 ^{+1.86} _{-5.43}	34.45 ^{+2.0} _{-1.8}	14.39 ^{+0.24} _{-0.24}	12.29 ^{+0.83} _{-0.23}
34.35 – 39.65	-1.90 ^{+0.05} _{-0.06}	-2.57 ^{+0.34} _{-7.43}	19.81 ^{+5.2} _{-7.6}	6.38 ^{+0.19} _{-0.16}	4.99 ^{+0.55} _{-0.62}
39.65 – 44.65	-2.01 ^{+0.04} _{-0.04}	3.47 ^{+0.15} _{-0.15}	3.50 ^{+0.30} _{-0.29}
44.65 – 49.65	-1.87 ^{+0.05} _{-0.05}	1.95 ^{+0.12} _{-0.13}	2.85 ^{+0.31} _{-0.31}
49.65 – 54.65	-2.06 ^{+0.08} _{-0.08}	1.50 ^{+0.13} _{-0.13}	1.30 ^{+0.26} _{-0.23}
54.65 – 59.65	-2.14 ^{+0.11} _{-0.12}	1.17 ^{+0.13} _{-0.12}	0.82 ^{+0.25} _{-0.22}
59.65 – 64.65	-2.36 ^{-0.14} _{+0.16}	0.93 ^{+0.12} _{-0.12}	0.35 ^{+0.16} _{-0.12}

Note. — Fluxes are in units of 10^{-7} erg/cm²/s. ^a α is the Band α parameter for those time regions where a Band β value is specified; otherwise, it is the index for a simple power-law fit. ^b Only WXM data were used in the fit. All errors are 90%.

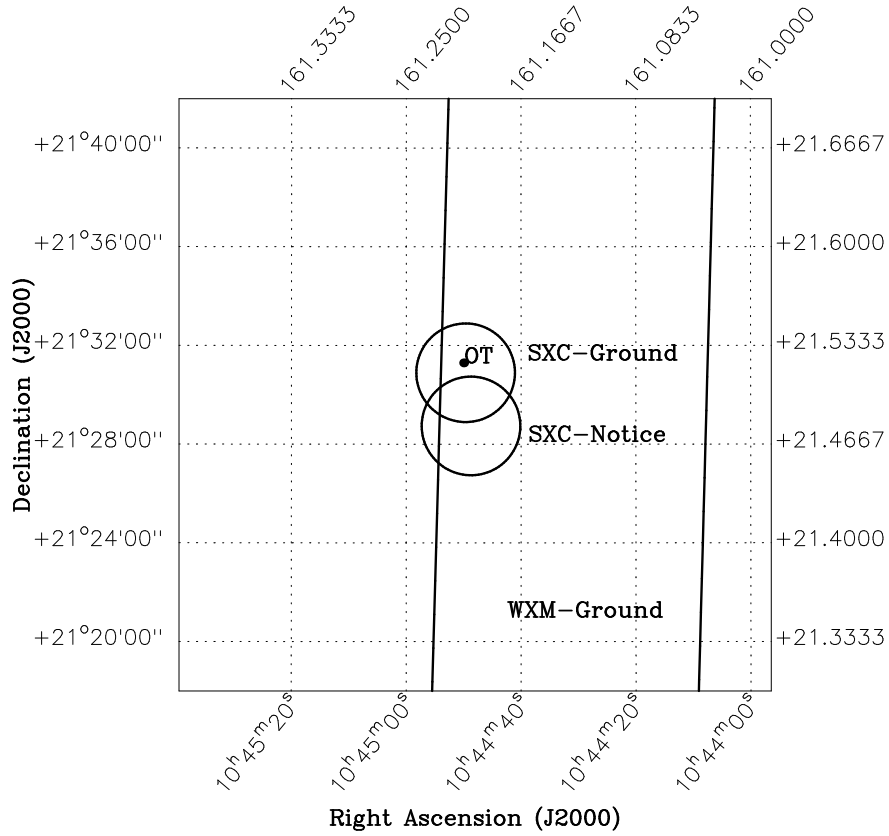


Fig. 1.— The localization history of GRB030329. Shown are a portion of the $12' \times 2.25^{\circ}$ WXM error region, the first SXC position (SXC-Notice), the SXC position corrected for the large systematic error at this burst’s incident angle (SXC-Ground), and the location of the OT. The SXC error regions are $2'$ in radius (90%).

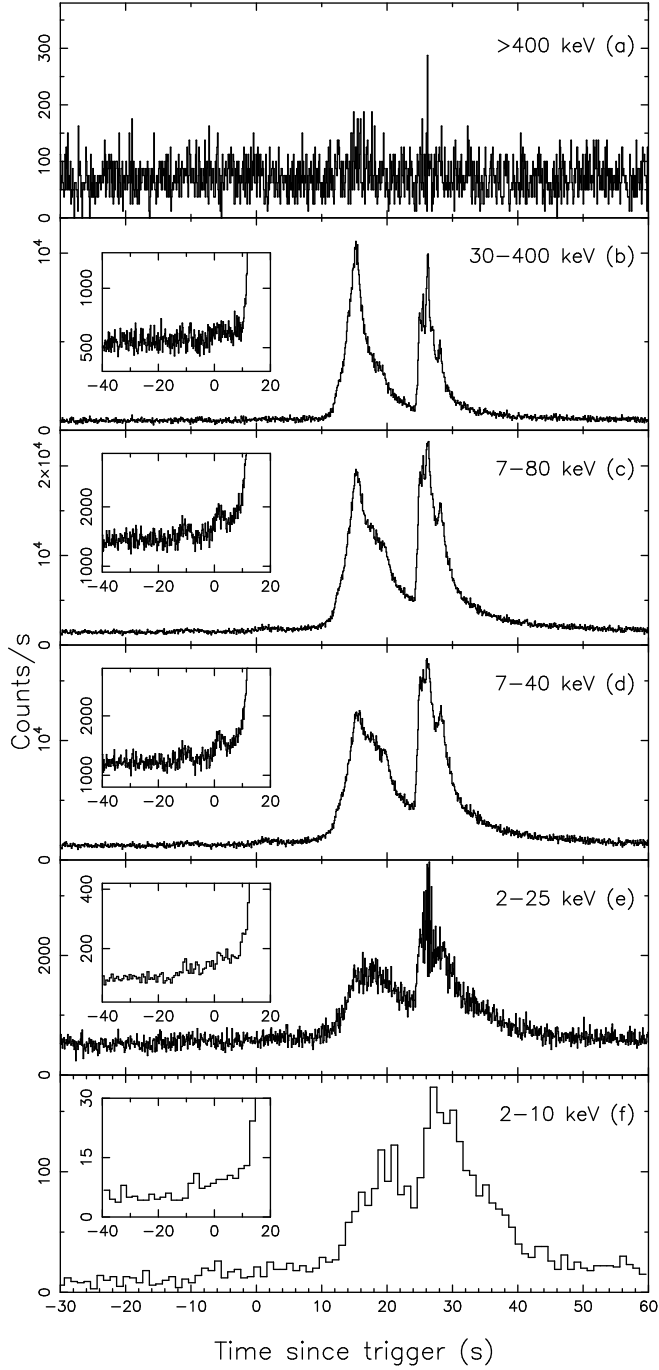


Fig. 2.— Time histories of GRB030329. Shown are the lightcurves in (a) Fregate band D, (b) Fregate band C, (c) Fregate band B, (d) Fregate band A, (e) the WXM, and (f) the SXC. The inset figures show more detail for the burst precursors in each band. The time resolution of the Fregate plots is 80 ms (160 ms in the insets); for the WXM, it is 80 ms (640 ms); for the SXC, it is 1 s (2 s). The broad time bands may hide significant spectral evolution at the start of the second pulse: the short spike in band D at $t=26.2$ s indicates that the burst was harder for a brief period at the start of the second pulse.

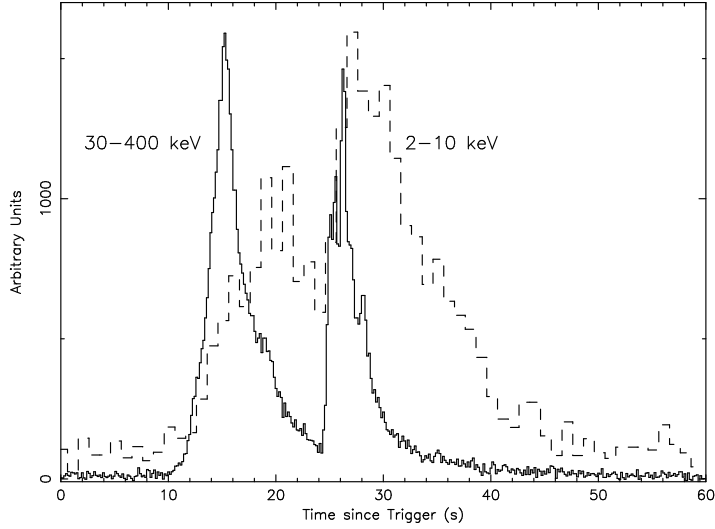


Fig. 3.— An overlay of the *Fregate* band C (30–400 keV; solid line) and *SXC* (2–10 keV; dashed line) lightcurves for GRB030329 show the distinct nature of the two pulses of GRB030329. There is a delay of ~ 5 seconds between the peak of the 30–400 keV and 2–10 keV emission in the first pulse, while the two are essentially simultaneous in the second pulse. (The *SXC* lightcurve has been scaled for clarity).

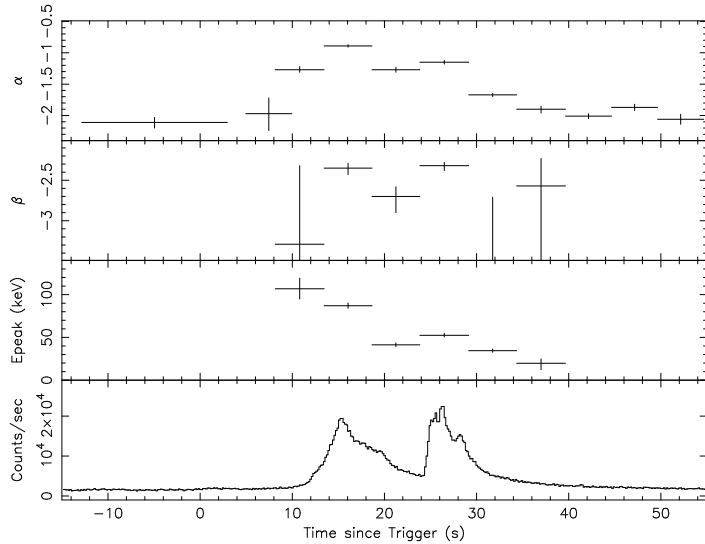


Fig. 4.— Variation of the spectral parameters of GRB030329 with time. Shown are the Band α , β , and E_{peak} parameters with the band B lightcurve for reference; for regions where Band β cannot be calculated, α is the index in a fit of a power law to the counts spectrum.

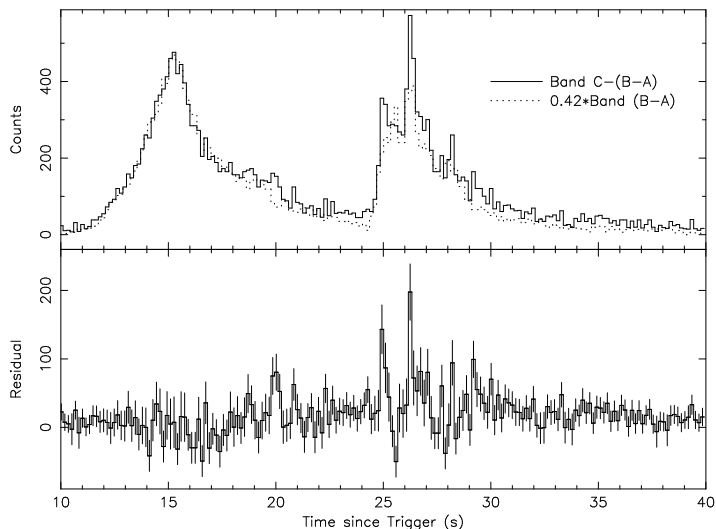


Fig. 5.— The 40–80 keV lightcurve of GRB030329, calculated as Fregate band B - Fregate band A, is scaled to the 30–400 keV minus the 40–80 keV lightcurve using a one-second interval centered on the peak of the first pulse ($t=14.5$ to $t=15.5$). The 40–80 keV lightcurve is multiplied by the ratio of the counts fluence in that time period (0.42) and compared to the band C-(B-A) lightcurve. The two lightcurves are shown in the upper panel: the solid line is band C-(B-A), the dotted line is $0.42 \cdot \text{band}(B-A)$. The difference between the two (lower panel) reflects excesses in either the 30–40 keV or the 80–300 keV band with respect to the template defined by the B-A lightcurve. The difference is consistent with zero except for a peak at $t=20$ s (coincident with the peak of the soft X-ray emission in the first pulse), two short spikes - - at $t=25$ s (coincident with the onset of the second pulse) and $t=26.2$ s (coincident with the spike in band D) - - and a faint extended tail starting at about $t=28$ s (consistent with an extended soft tail to the burst). We conclude that the overall shape of the lightcurve of GRB030329 does not vary significantly from 30 to 400 keV, and thus that the soft X-ray pulse seen in Figure 3 could be due to a different emission mechanism than the main burst.